ORIGINAL PAPER

Redox induced dual-signal optical sensor of carbon dots/MnO₂ nanosheets based on fluorescence and second-order scattering for the detection of ascorbic acid

Qian Tang[1] · Yu Zhu Fan[1] · Lei Han[1] · Yu Zhu Yang[1] · Nian Bing Li[1] · Hong Qun Luo[1]

Abstract

In order to detect ascorbic acid (AA) sensitively, a dual-signal optical sensor of a nanosystem with carbon dots (CDs)/MnO₂ nanosheets based on fluorescence and second-order scattering (SOS) has been constructed. Here, MnO₂ nanosheets, both as a fluorescence quencher and signal transducer of SOS, quench the blue fluorescence of CDs by an inner filter effect. Under the excitation of 300 nm, the nanosystem shows a fluorescence emission peak at 405 nm and a SOS peak at 610 nm, respectively. With the increase of AA , the lamellar structure of MnO₂ nanosheets is etched into a smaller nanostructure, causing a decrease of the fluorescence recovery of CDs (405 nm) and decrease of the SOS signal of the MnO₂ nanosheets (610 nm). According to the simultaneous changes of fluorescence and SOS signals, a dual-signal optical sensor toward AA is successfully constructed. Satisfactorily, the optical sensor for AA detection shows a detection limit of 88 and 105 nM for fluorescence and SOS, respectively. The practical application of the designed sensor is verified through the detection of AA content in vitamin C tablets, and satisfactory results are obtained

Keywords Nanosystem · Dual-signal sensor · Ascorbic acid · Second-order scattering · Fluorescence

Introduction

As an antioxidant biomolecule, ascorbic acid (AA) is essential for maintaining human life, mainly by participating in the regulation of body metabolism [1]. Insufficient AA will lead to bleeding, scurvy, and other diseases, while excessive AA may induce some diseases such as urinary stones, gastro spasms, and others [2, 3]. In consequence, it is significant to design a rapid and sensitive sensor for AA detection.

Up to now, there have been many methods developed to track AA, such as fluorescence [4], electrochemistry [5], electrochemiluminescence [6], colorimetry [7], chromatography [8], and others [9], among which the fluorescence method was widely used due to its high sensitivity, simple operation, and easy access to equipment [10]. In the above methods, however, most of them are single-signal detectors, whose accuracy and reliability are much lower than those of dual-signal sensors. Accordingly, it would be of great significance to develop a dual-signal detector for the sensitive and highly accurate detection of AA.

As an environmentally friendly fluorescence probe, carbon dots (CDs) show excellent performance in having low toxicity, photostability, and low cost, so they have been widely applied in different categories of analyte detection [11, 12]. On the other hand, MnO₂ nanosheets show a wide application prospect as fluorescence quenchers on account of their large surface areas and excellent light absorption properties [13, 14].

In recent years, sensing platforms comprising two or more nanomaterials have been widely explored, one of which was used as the fluorescent donor and other as the fluorescence quencher [15, 16]. For instance, Chen et al. designed a "switch-on" fluorescence approach for sensing of AA, in

✉ Nian Bing Li
linb@swu.edu.cn

✉ Hong Qun Luo
luohq@swu.edu.cn

[1] Key Laboratory of Eco-Environments in Three Gorges Reservoir Region (Ministry of Education), School of Chemistry and Chemical Engineering, Southwest University, Chongqing 400715, People's Republic of China

which the fluorescence intensity of CDs was first quenched by the addition of MnO$_2$ nanosheets and then recovered due to the redox reaction between AA and MnO$_2$ nanosheets [17]. Obviously, good progress has been made in the detection of analytes by fluorescence recovery using nanocomposites, such as low detection limit and wide linear range. However, there are still some deficiencies in these methods, like susceptible, insufficient accuracy and other problems. Dual-signal sensors, with two independent output modes, can improve the accuracy of detection since the two signals do not interfere with each other [18]. And some researches on the combination of two different signal outputs, such as fluorescence and UV-vis absorption [19, 20], for analytical detection have attracted people's attention. Unsatisfactorily, these methods need to be tested by two kinds of instruments, respectively, which greatly increase the difficulty and complexity of the experimental operation. The combination of fluorescence and scattering not only improves the accuracy of sensing but also provides two signals simultaneously under the same excitation, which lays the foundation for simple experiments. Therefore, it is still essential to design a dual-signal sensor, which is simple and easy to prepare, accurate, and sensitive.

Herein, a dual-signal fluorescence (FL) and second-order scattering (SOS) optical sensor based on the CD/MnO$_2$ nanosystem was created for AA detection. As illustrated in Scheme 1, MnO$_2$ nanosheets were added to a CD solution and both were hybridized together to form a dual-signal probe. It was found that the fluorescence of CDs (405 nm) was quenched by MnO$_2$ nanosheets via an inner filter effect (IFE). And MnO$_2$ nanosheets provided a strong SOS signal (610 nm) due to the large surface area. Interestingly, MnO$_2$ can be reduced to Mn^{2+} because of the reducibility of AA. Therefore, MnO$_2$ nanosheets were etched into smaller nanoparticles after adding AA, causing the weakening of the SOS signal and the fluorescence recovery of CDs. According to the

above mechanism, a highly accurate, highly sensitive, and simple dual-signal detector was constructed via collecting fluorescence and SOS signals simultaneously. At last, the detector was successfully applied to the detection of AA in vitamin C tablets.

Experimental section

Synthesis of CDs and MnO$_2$ nanosheets

CDs were synthesized by a simple hydrothermal method on the basis of a previously reported article with a minor modification [21]. And MnO$_2$ nanosheets were prepared by an oxidation approach based on a previous paper published by our group with a minor modification [22]. The detailed synthesis steps are displayed in the synthetic section of the Supporting Information.

Detection of AA

For the dual signal of fluorescence and SOS detection of AA, 1.0 mL of twofold-diluted CDs and 2.0 mL of sixfold-diluted MnO$_2$ nanosheets were stirred as the probe. And 30 μL of the as-prepared probe, 500 μL of ultrapure water, and 100 μL of Na$_2$HPO$_4$-KH$_2$PO$_4$ buffer (PB, 1/15 M, pH = 7.0) were mixed together. Subsequently, 10 μL of different concentrations of AA solution was added to the above mixture. Then the mixed solutions were stirred for 1 min and reacted for 10 min at room temperature. Finally, the fluorescence (405 nm) and SOS signals (610 nm) of the analyte were obtained at 300 nm excitation. For the final results, three groups of parallel samples were measured and their average values were taken.

Scheme 1 Principle of fluorescence and SOS based on the CD and MnO$_2$ nanosheet system for the AA detection
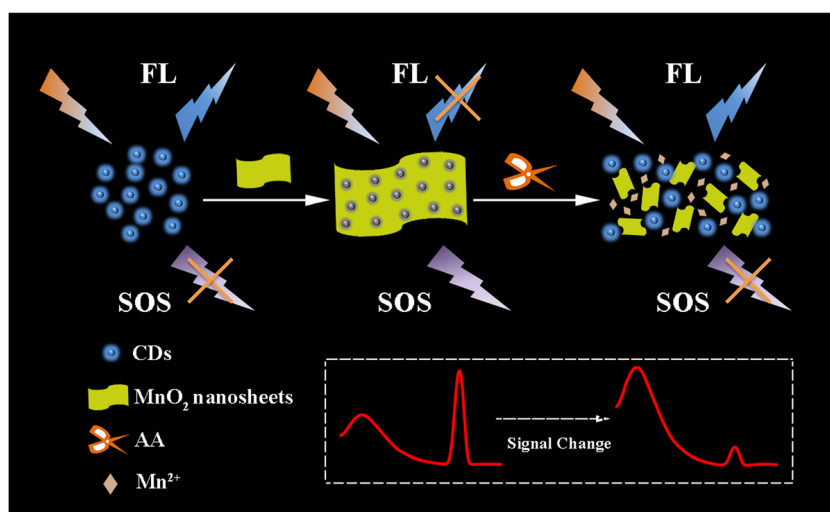
Application to real sample

Vitamin C tablets were purchased from Huazhong Pharmaceutical Co., Ltd. The process of sample preparation and testing was as follows: Vitamin C tablets were pestled into fine powder in a quartz bowl and dissolved with ultrapure water to obtain 0.1 mg mL^{-1} sample solution. And 30 μL of the as-prepared probe, 500 μL of ultrapure water, 100 μL of PB buffer (1/15 M, pH = 7.0), and 12 μL of sample solution were mixed together. The fluorescence signal at 405 nm and SOS signal at 610 nm of the mixture solution were then collected under the excitation of 300 nm. In addition, the sample solution with the addition of different levels of AA (5, 10, 20 μM) was treated by the same procedure mentioned above to obtain the fluorescence signal (405 nm) and SOS signal (610 nm) under the same excitation. For the final results, three groups of parallel samples were measured and their average values were taken.

Results and discussion

Characterization of CDs and MnO$_2$ nanosheets

CDs were synthesized via a facile one-pot hydrothermal method using aminobenzene boric acid as a raw material. The TEM image in Fig. 1a and the size distribution in Fig. S1 indicate that CDs exhibit good monodispersity with an average diameter of 2.7 nm. The high-resolution transmission electron microscope (HRTEM) image of CDs (inset of Fig. 1a) demonstrates that the lattice spacing of CDs is approximately 0.21 nm, which is ascribed to the in-plane lattice spacing of a graphene structure (100 facet) [23]. Meanwhile, the fluorescence quantum yield (QY) of CDs was measured to be 4.4% according to a slope method. And the detailed measurement procedure is described in the Supporting Information. As exhibited in the UV-vis absorption spectrum (Fig. 1c), it is obvious that the CD solution reveals two specific absorption peaks at 229 and 277 nm. The characteristic peak at 229 nm is attributed to n-π* transition of C=C–N [24], and another specific peak at 277 nm is the consequence of π-π* transition of the C=C bond [25]. The inset in Fig. 1c shows that the CD solution is yellowish under visible light and emits bright blue fluorescence under UV light (302 nm). The above experimental characterization proved the successful synthesis of CDs. Furthermore, the fluorescence properties of the CDs were also analyzed in detail. As revealed in Fig. S2 and Fig. 1c, the fluorescence spectra of CDs reveal two emission peaks at 340 and 405 nm with the range of excitation wavelength between 270 and 360 nm, whose maximum excitation wavelengths are 280 and 300 nm. In order to observe the change of CD fluorescence with the naked eye, which is useful for the simple experiments, 300 nm was used as the excitation wavelength for subsequent experiments.

The UV-vis absorption spectrum of the MnO$_2$ nanosheet solution in Fig. 1d exhibits an excellent light absorption performance in the range of 200–600 nm, which reveals a specific center at 365 nm. Satisfactorily, the above spectral characterization demonstrates the successful preparation of MnO$_2$ nanosheets [26]. In addition, the TEM
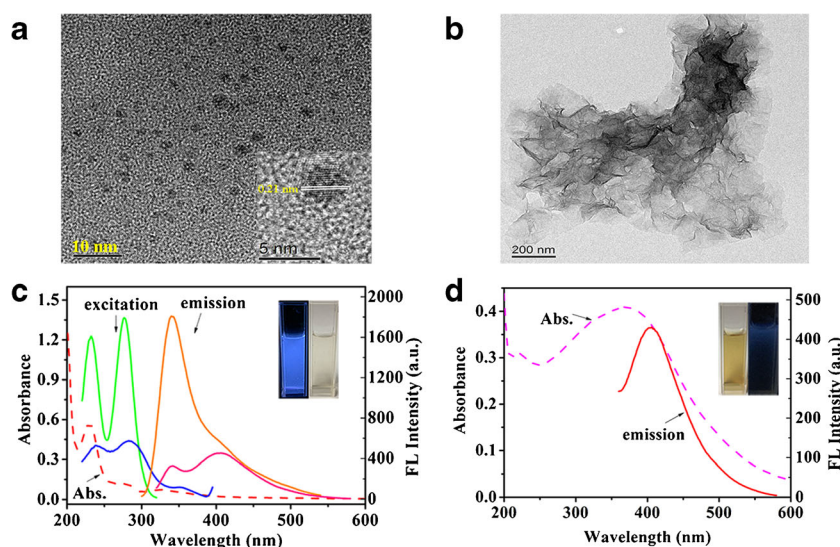

Fig. 1 a TEM image of CDs. The inset displays the HRTEM image. **b** TEM image of MnO$_2$ nanosheets. **c** UV-vis absorption (red dashed line), fluorescence excitation (green and blue solid lines), and fluorescence emission (orange and pink solid lines) spectra of CDs. Insets are photographs of CD solution under UV light of 302 nm (left) and visible light (right). Conditions: $C_{(CDs)}$ = 17 μL/mL. **d** Emission spectrum of CDs and absorption spectrum of MnO$_2$ naonosheets. Insets are photographs of CD and MnO$_2$ nanosheet solutions in visible light (left) and 302 nm UV light (right). Conditions: $C_{(CDs)}$ = 17 μL/mL; $C_{(MnO2)}$ = 34 μL/mL

image of MnO_2 nanosheets (Fig. 1b) indicates that the MnO_2 nanosheets have a lamellar structure with wrinkles and a size of hundreds of nanometers. The AFM image of the MnO_2 nanosheets (Fig. S3) further shows the ultrathin monolayer structure of the MnO_2 nanosheets, with a thickness of about 0.8 nm.

Design strategy of the dual-signal optical sensor

In order to obtain the optical sensor with dual signals of fluorescence and scattering, the fluorescent materials and fluorescence quenchers with large size were required. And CDs were chosen as the fluorescent material for the optical sensor since they show the advantages of low toxicity and simple synthesis compared with traditional fluorescent dyes and quantum dots [11, 12]. Furthermore, the sensor was used to detect AA by redox reaction, so MnO_2 nanosheets with oxidation properties were required. More importantly, MnO_2 nanosheets show an excellent absorption property with large surface area, which were used as the fluorescence quencher and the SOS signal donor. In addition, since the zeta potential measured in CDs and MnO_2 nanosheets was − 11.5 and − 13.3 mV, respectively, both of which were negatively charged,

electrostatic repulsion existed between them. On the other hand, the surface of CDs contained abundant functional groups, such as –COOH, C=O, –OH, –NH, etc. [25], and the FT-IR spectrum of MnO_2 nanosheets indicated that they had a Mn–O bond [26], so it is speculated that CDs and MnO_2 nanosheets may have hydrogen bonding in aqueous solution. To demonstrate the quenching mechanism of CD fluorescence by MnO_2 nanosheets, the light absorption property of CDs and MnO_2 nanosheets, the emission spectrum of CDs, and the fluorescence lifetime variation were collected. As exhibited in Fig. 2a, the addition of MnO_2 nanosheets has no influence on the fluorescence lifetime of CDs. Therefore, it is inferred that the quenching mechanism could not be dynamic quenching, photo-induced electron transfer (PET), or fluorescence resonance transfer (FRET), whose fluorescence intensity changes will be accompanied by change in fluorescence lifetime [27]. Moreover, it can be observed that no characteristic peaks appeared in the UV-visible absorption spectra of CDs with the addition of MnO_2 nanosheets (Fig. S4). So it can be inferred that the quenching mechanism is not static quenching [28]. Additionally, as shown in Fig. 1d, MnO_2 nanosheets show a wide absorption band ranging from 200 to 600 nm, which overlaps well
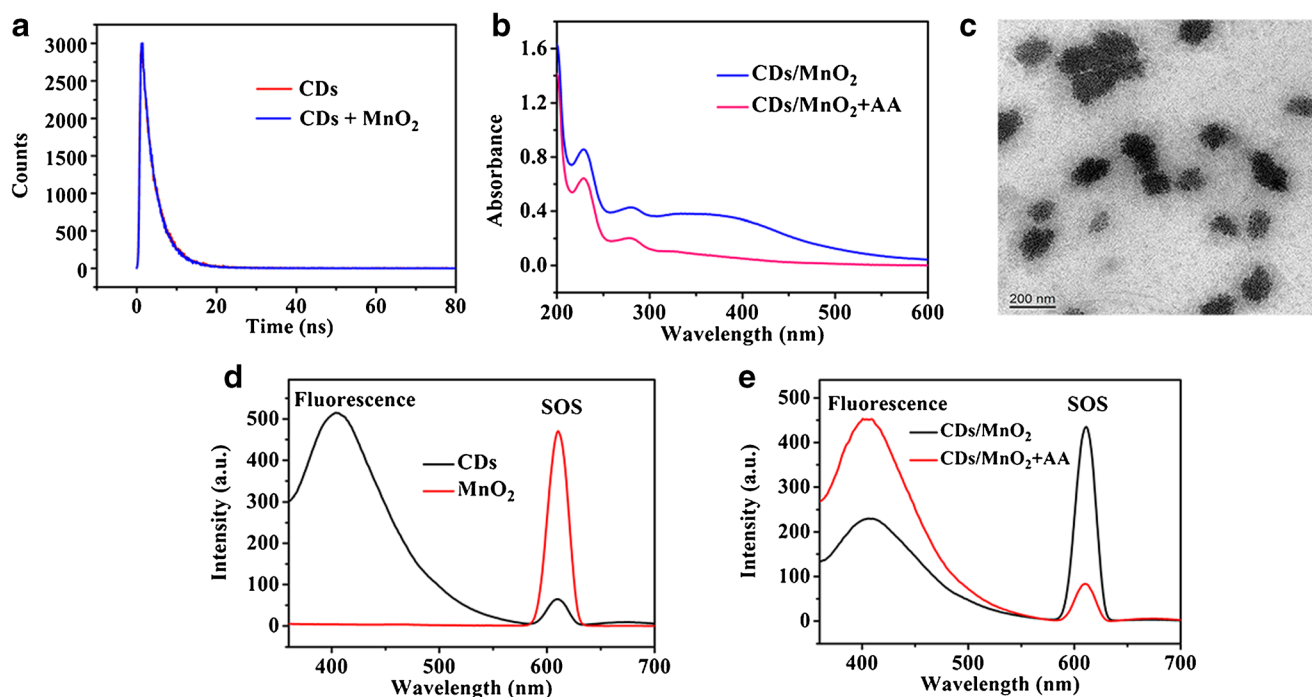

Fig. 2 a Time-resolved decay of CDs (red line) and CDs with MnO_2 nanosheets (blue line), respectively. b UV-vis absorption spectra of the CD and MnO_2 system in the presence and absence of 35 μM AA, respectively. Conditions: PB buffer (1/15 M, pH = 7.0); $C_{(CDs)}$ = 17 μL/mL; $C_{(MnO2)}$ = 34 μL/mL. c TEM image of MnO_2 nanosheets with the addition of 35 μM AA. d Fluorescence and SOS spectra of CDs and MnO_2 nanosheets. Conditions: PB buffer (1/15 M, pH = 7.0); $C_{(CDs)}$ = 17 μL/mL; $C_{(MnO2)}$ = 34 μL/mL. e Fluorescence and SOS spectra of the CD and MnO_2 nanosheet system in the presence and absence of 35 μM AA, respectively. Conditions: PB buffer (1/15 M, pH = 7.0); $C_{(CDs)}$ = 17 μL/mL; $C_{(MnO2)}$ = 34 μL/mL

with the emission spectrum of CDs. Consequently, the mechanism of MnO_2 nanosheets quenching CD fluorescence is an inner filter effect (IFE) [29, 30].

From Rayleigh scattering theory, the size of nanomaterials greatly restricts its scattering intensity under certain conditions. (Eq. 1) [31]:

$$I = \frac{8\pi^4 a^6 n^4 I_0}{r^2 \lambda_0^4} \left| \frac{m^2-1}{m^2+2} \right|^2 (1+\cos\theta)^2 \tag{1}$$

where a represents the scatterer radius; n denotes the refractive index of the medium; I_0 and λ_0 are the intensity and wavelength of the excitation light, respectively; r is the distance between the detector and scatterer as the crow flies; m signifies the relative refractive index of the scatterer; and θ is the included angle of the incident light and the detector. The aggregation, dispersion, and corrosion of nanomaterials can change their size and morphology, consequently leading to the evolution of scattering intensity.

In addition, according to the Fraunhofer single-slit diffraction principle, SOS, as the diffraction peak of Rayleigh scattering, is mainly determined by the properties of the analytes, except for the instrument, measuring conditions, and medium. And the intensity of diffracted light is expressed by the following formula (Eq. 2) [32]:

$$I = I_0 \left[\frac{\sin\left(\frac{\pi w}{\lambda}\sin\theta\right)}{\frac{\pi w}{\lambda}\sin\theta} \right]^2 \tag{2}$$

where I_0 is the light intensity at the center of the pattern, w is the width of the slit, λ is the excitation wavelength, and θ is the angle of rotation. Evidently, the intensity of diffracted light is largely determined by the intensity of central light but exhibits much weaker at the same time. As a consequence, the SOS intensity is closely related to the intensity of Rayleigh scattered light, so its intensity is also relevant to the size of materials.

Based on the above theories, a certain number of sensors have been developed, whose response signal was the scattering intensity [33, 34]. However, only a few studies have been reported on the simultaneous collection of fluorescence and SOS signals under the same excitation [31, 35]. Obviously, collecting the fluorescence and SOS signals at an excitation wavelength can endow the appealing simplification of operation. For the purpose of obtaining the fluorescence and SOS simultaneously, the fluorescence and SOS of CDs and MnO_2 nanosheets were explored, respectively. As depicted in Fig. 2d, when 300 nm was chosen as the excitation wavelength, MnO_2 nanosheets exhibit a strong SOS intensity at 610 nm, while there is no fluorescence intensity. On the contrary, CDs have an obvious fluorescence center at 405 nm with weak SOS. Next, the fluorescence and SOS intensity of the system were tested with CD/MnO_2 nanosheet composites as the probe, under the excitation of 300 nm in the presence and absence of AA, respectively. And it is clear that MnO_2 can be reduced to Mn^{2+} with the addition of AA according to Eq. 3, which has been further evidenced by Fig. 2b, showing that after addition of AA, the characteristic absorption band with a specific center at 365 nm of MnO_2 nanosheets disappears. In order to further illustrate that MnO_2 nanosheets were reduced to Mn^{2+} by AA, the XPS spectra of MnO_2 nanosheets in the absence and presence of AA were collected, respectively. As shown in Fig. 3a, the binding energy of Mn $2p_{3/2}$ located at around 639.6, 640.5, and 642.5 eV can be ascribed to Mn^{2+}, Mn^{3+}, and Mn^{4+}, respectively [20]. In addition, the XPS spectrum of Mn $2p_{3/2}$ showed obvious changes with the addition of AA, in which the peak value of Mn^{4+} decreased significantly, while the peak value of Mn^{2+} enhanced obviously (Fig. 3b). Additionally, AA etched the lamellar structure of MnO_2 nanosheets into smaller nanoparticles, which has been proved by comparison of Fig. 1b with Fig. 2c. Furthermore, the morphological changes of CDs@MnO_2 nanosystem were characterized by the TEM image (Fig. S5). Since CDs (2.7 nm) were too small to be observed compared to MnO_2 nanosheets, only the lamellar structure of MnO_2 nanosheets can be observed in the TEM image. And the TEM image of the CDs@MnO_2 nanosystem also confirms that MnO_2 nanosheets were etched into a smaller shape.

$$\text{(AA)} + MnO_2 + 2H^+ \longrightarrow \text{(DHA)} + Mn^{2+} + 2H_2O \tag{3}$$
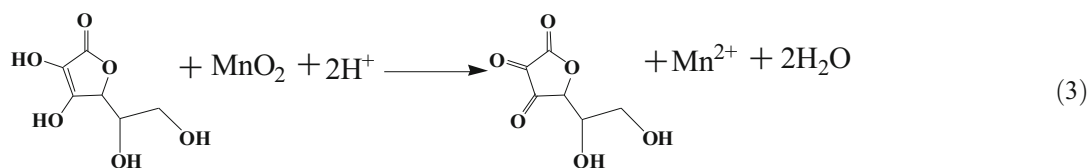
As a result, the SOS signal of MnO_2 nanosheets was strongly deprived. As expected, the CDs and MnO_2 composites emit weak fluorescence, however, with a strong SOS signal. Nevertheless, after the addition of AA, the fluorescence intensity of the system increases by degrees, whereas the SOS signal gradually decreases in Fig. 2e. It indicates that the CD/MnO_2 nanosheet dual-signal sensor for the AA

Fig. 3 XPS spectra of Mn $2p_{3/2}$ in MnO$_2$ nanosheets in the absence (**a**) and presence (**b**) of 50 μM AA, respectively
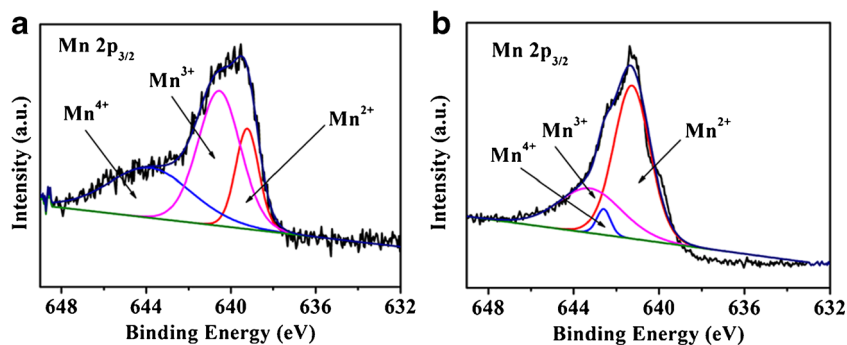
detection was constructed successfully using the simultaneous response of fluorescence and SOS.

Detection of AA with the dual-signal optical sensor

In order to maximize the property of the dual-signal optical sensor, the ratio of CDs to MnO$_2$ nanosheets, reaction pH, and reaction time were optimized before the detection. As illustrated in Fig. 4, with the increase of the MnO$_2$ nanosheet content, the fluorescence intensity of CDs decreases gradually, while the SOS intensity increases sharply first and then decreases slightly. Obviously, when the added volume of MnO$_2$ nanosheets reaches 20 μL, the SOS intensity reaches a maximum value. Considering both of the fluorescence and SOS peaks, the optimal volumes of MnO$_2$ and CDs were 20 and 10 μL for the whole article, respectively. Furthermore, the influence of pH on AA monitoring was investigated using PB buffers with a pH range of 6.5–9.0. As depicted in Fig. S6A, when the reaction pH is 7.0, the value of $F/F_0 - 1$ reaches a maximum value and the value of $F/F_0 - 1$ gradually decreases as the pH increases, where F and F_0 represent the fluorescence intensity of the CD and MnO$_2$ system in the presence and absence of AA, respectively. It is speculated that the
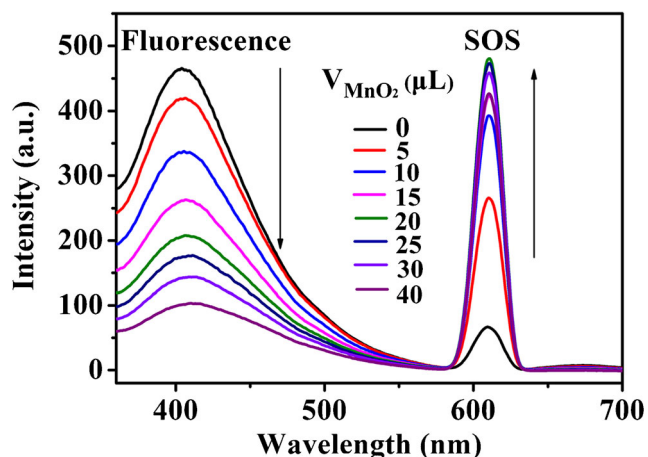
fluorescence of CDs will be quenched partly under alkaline conditions, which is coincident with the former research achievements [21]. As shown in Fig. S6B, however, the value of S/S_0 is substantially constant in the range of pH 6.5–7.5, and gradually increases in the range of 7.5–9.0, where S and S_0 represent the SOS intensity of the CD and MnO$_2$ system in the presence and absence of AA, respectively. Thus, reaction pH 7.0 was selected as the optimal pH in the following experiments. Finally, both of the fluorescence and SOS intensity have no significant change when the reaction time reaches 10 min in Fig. S6C and Fig. S6D. In conclusion, the optimal conditions for AA detection are as follows: a volume ratio of MnO$_2$ nanosheets to CDs is 20 μL/10 μL, the pH value is 7.0, and the reaction time is 10 min.

Under the optimal experimental conditions, the linear response range, limit of detection (LOD), and selectivity of AA detection were evaluated by using the dual-signal optical probe. As indicated in Fig. 5a, the fluorescence intensity gradually increases, while the SOS intensity gradually decreases with the increase of AA concentration. Moreover, Fig. 5b and Fig. 5c display that fluorescence and SOS signal changes of the probe have a good linear relationship with the AA concentration in the range of 0.2–40 μM ($R^2 = 0.998$ for the fluorescence mode, $R^2 = 0.996$ for the SOS mode), displaying a relatively wide linear range. In addition, the ratiometric technique was also used to determine the value of AA, but the linear range obtained was too narrow to be suitable for practical application. Consequently, we chose to use two independent signals, fluorescence and SOS, to detect AA. Finally, on the basis of $S/N = 3$, the LOD of AA was calculated to be 88 and 105 nM based on fluorescence and SOS modes, respectively. And it can be seen that there is almost no difference between the two LOD values, which is more significant to use the dual-signal probe to detect real samples. Compared to the previous methods of AA detection (Table S1), this method can output double signals at the same time with higher accuracy and sensitivity. For the practicality of the sensor, good selectivity is also desired. Therefore, the influence of some substances was tested by using the dual-signal optical sensor, including some similar reductive substances (DA, Cys, GSH), different sugars (Glu, Fru, Suc, and Mal), some
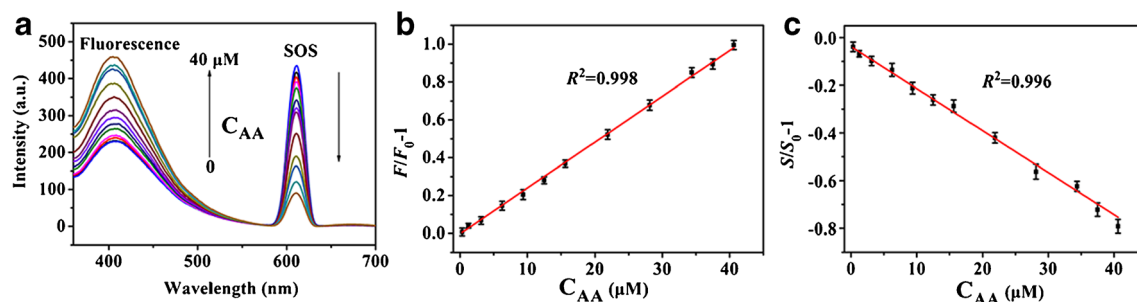

Fig. 4 Fluorescence and SOS spectra of the CD and MnO$_2$ nanosheet system with the addition of different volumes of MnO$_2$ nanosheets. Conditions: PB buffer (1/15 M, pH = 7.0); $V_{(CDs)} = 10$ μL

Fig. 5 **a** Fluorescence and SOS spectra of the CD and MnO$_2$ nanosheet system with different concentrations of AA. The corresponding linear plots indicate the relationship of $F/F_0 - 1$ (**b**) and $S/S_0 - 1$ (**c**) to the AA concentration in the range of 0.2–40 μM (0.2, 1.5, 3.5, 6.5, 9.5, 12.5, 15.5, 21.5, 28.5, 34.5, 37.5, 40 μM), respectively. Conditions: PB buffer (1/15 M, pH = 7.0); $C_{(CDs)}$ = 17 μL/mL; $C(MnO_2)$ = 34 μL/mL

common cations (K$^+$, Na$^+$, Ca^{2+}, Mg^{2+}, and Zn^{2+}), some common anions (Cl$^-$, Br$^-$, CO$_3^{2-}$, SO$_4^{2-}$, and NO$_3^-$), and other common substances (CA, Dex, Gly, and Ala). It can be observed from Fig. S7C and Fig. S7D that other common reductive substances (DA, Cys, GSH) had certain influence on the detection of AA. However, they are not as reductive as AA. In addition, for other substances, including some cations, anions, common sugars, and common species, the fluorescence and SOS intensity changes of the sensor were negligible compared with AA (Fig. S7). Thus, this method has good selectivity for AA monitoring.

Detection of AA in vitamin C tablets

The feasibility and practicability of the dual-signal sensor were verified by detecting the content of AA in vitamin C tablets. The commercial vitamin C tablets were measured by the above modus, and the consequences are presented in Table 1. It can be observed that the recoveries of AA based on fluorescence mode are in the range of 93.4–100.8% in vitamin C tablets, and the recoveries are in the range of 96.6–104.5% with SOS assay. Satisfactorily, the content of AA in the tablet was 97.5% for fluorescence assay and 106.0% for SOS assay. And both of them were within the allowable range of 93.0–107.0% according to the standards of the 2015 edition of the *Chinese Pharmacopoeia*. Furthermore, the recoveries of the two signals are basically

the same, which prove that the dual-signal sensor has potential application in actual sample analysis and detection.

Conclusions

An uncomplicated and sensitive AA detection system with fluorescence and SOS double-signal output has been successfully constructed, in which CDs were used as the fluorescence donor, and MnO$_2$ nanosheets as the fluorescence quencher and SOS signal donor. Because of the large surface areas and great light absorption properties, MnO$_2$ nanosheets can skillfully quench the CD fluorescence via IFE. After the combination of MnO$_2$ nanosheets and CDs, the fluorescence turns off whereas the new SOS appears. With the addition of reductive AA, MnO$_2$ nanosheets were etched into a smaller nanostructure. This results in the recovery of the fluorescence of CDs and decrease of the SOS signal, which can achieve dual-signal detection of AA. The dual-signal sensor has the advantages of high sensitivity, good selectivity, and wide detection range. And most importantly, it has higher accuracy than the common single-signal sensors. Finally, the dual-signal sensor has been successfully used to detect the AA content of vitamin C tablets. This study not only provides a new method to detect AA but also extends the utilization of the SOS technique.

Compliance with ethical standards

Conflict of interest The authors declare that they have no competing interests.

Table 1   Detection of AA in vitamin C tablets ($n = 3$)

Sample	Added (μM)	Total found (μM)		Recovery (%)	
		FL	SOS	FL	SOS
1	0	10.35 ± 0.34	11.25 ± 0.11	–	–
2	5	15.02 ± 0.49	16.08 ± 0.17	93.40	96.60
3	10	20.08 ± 0.75	21.70 ± 0.39	97.30	104.50
4	20	30.50 ± 0.50	31.05 ± 0.25	100.75	99.00

References

1. Hou X, Zhan G, Huang X, Wang N, Ai Z, Zhang L (2019) Persulfate activation induced by ascorbic acid for efficient organic

pollutants oxidation. Chem Eng J 382:122355. https://doi.org/10.1016/j.cej.2019.122355

2. Yang YJ, Jo A, Lee YM, Lee CM (2018) Electrodeposited nanoporous ruthenium oxide for simultaneous quantification of ascorbic acid and uric acid using chronoamperometry at two different potentials. Sensors Actuators B Chem 255:316–324. https://doi.org/10.1016/j.snb.2017.08.089

3. Zhang LM, Qin J, Yang Q, Wei SQ, Yang R (2019) Redox modulated fluorometric sensing of ascorbic acid by using a hybrid material composed of carbon dots and CoOOH nanosheets. Microchim Acta 186:368–374. https://doi.org/10.1007/s00604-019-3483-9

4. Li N, Li YH, Han YY, Pan W, Zhang TT, Tang B (2014) A highly selective and instantaneous nanoprobe for detection and imaging of ascorbic acid in living cells and in vivo. Anal Chem 86:3924–3940. https://doi.org/10.1021/ac5000587

5. Barberis A, Spissu Y, Bazzu G, Fadda A, Azara E, Sanna D, Schirra M, Serra PA (2014) Development and characterization of an ascorbate oxidase-based sensor-biosensor system for telemetric detection of AA and antioxidant capacity in fresh orange juice. Anal Chem 86:8727–8734. https://doi.org/10.1021/ac502066a

6. Wang H, Pu GQ, Devaramani S, Wang YF, Yang ZF, Li LF, Ma XF, Lu XQ (2018) Bimodal electrochemiluminescence of G-CNQDs in the presence of double coreactants for ascorbic acid detection. Anal Chem 90:4871–4877. https://doi.org/10.1021/acs.analchem.8b00517

7. Porto ISA, Santos Neto JH, dos Santos LO, Gomes AA, Ferreira SLC (2019) Determination of ascorbic acid in natural fruit juices using digital image colorimetry. Microchem J 149:104031. https://doi.org/10.1016/j.microc.2019.104031

8. Li XN, Franke AA (2009) Fast HPLC-ECD analysis of ascorbic acid, dehydroascorbic acid and uric acid. J Chromatogr B 877:853–856. https://doi.org/10.1016/j.jchromb.2009.02.008

9. Bazel Y, Riabukhina T, Tirpák J (2018) Spectrophotometric determination of ascorbic acid in foods with the use of vortex-assisted liquid-liquid microextraction. Microchem J 143:160–165. https://doi.org/10.1016/j.microc.2018.08.003

10. Guo L, Liu Y, Kong RM, Chen G, Liu Z, Qu FL, Xia L, Tan WH (2019) A metal-organic framework as selectivity regulator for $Fe^{(3+)}$ and ascorbic acid detection. Anal Chem 91:12453–12460. https://doi.org/10.1021/acs.analchem.9b03143

11. Sidhu JS, Singh A, Garg N, Kaur N, Singh N (2019) Gold conjugated carbon dots nano assembly: FRET paired fluorescence probe for cysteine recognition. Sensors Actuators B Chem 282:515–522. https://doi.org/10.1016/j.snb.2018.11.105

12. Wang YL, Lao SY, Ding WJ, Zhang ZD, Liu SY (2019) A novel ratiometric fluorescent probe for detection of iron ions and zinc ions based on dual-emission carbon dots. Sensors Actuators B Chem 284:186–192. https://doi.org/10.1016/j.snb.2018.12.139

13. Peng C, Xing HH, Fan XS, Xue Y, Li J, Wang E (2019) Glutathione regulated inner filter effect of MnO_2 nanosheets on boron nitride quantum dots for sensitive assay. Anal Chem 91:5762–5767. https://doi.org/10.1021/acs.analchem.8b05961

14. Zhu SM, Wang SC, Xia MM, Wang BJ, Huang Y, Zhang DX, Zhang XJ, Wang GF (2019) Intracellular imaging of glutathione with MnO_2 Nanosheet@Ru(bpy)$_3$$^{(2+)}$-UiO-66 nanocomposites. ACS Appl Mater Interfaces 11:31693–31699. https://doi.org/10.1021/acsami.9b11025

15. Wang J, Peng X, Li DQ, Jiang XC, Pan ZF, Chen AM, Huang L, Hu J (2018) Ratiometric ultrasensitive fluorometric detection of ascorbic acid using a dually emitting CdSe@SiO$_2$@CdTe quantum dot hybrid. Microchim Acta 186:42–50. https://doi.org/10.1007/s00604-017-2557-9

16. Achadu OJ, Revaprasadu N (2019) Tannic acid-derivatized graphitic carbon nitride quantum dots as an "on-off-on" fluorescent nanoprobe for ascorbic acid via copper (II) mediation. Microchim Acta 186:87–96. https://doi.org/10.1007/s00604-018-3203-x

17. Liu JJ, Chen YL, Wang WF, Feng J, Liang MJ, Ma SD, Chen XG (2016) "Switch-on" fluorescent sensing of ascorbic acid in food samples based on carbon quantum dots-MnO_2 probe. J Agric Food Chem 64:371–380. https://doi.org/10.1021/acs.jafc.5b05726

18. Lin X, Hai X, Wang N, Chen XW, Wang JH (2017) Dual-signal model array sensor based on GQDs/AuNPs system for sensitive protein discrimination. Anal Chim Acta 992:105–111. https://doi.org/10.1016/j.aca.2017.09.006

19. Liu SG, Han L, Li N, Ju YJ, Li NB, Luo HQ (2018) Fluorescent and colorimetric dual-mode assay of alkaline phosphatase activity via destroying oxidase-like CoOOH nanoflakes. J Mater Chem B 6:2843–2850. https://doi.org/10.1039/C7TB03275G

20. Han L, Liu SG, Liang JY, Li NB, Luo HQ (2019) Free-label dual-signal responsive optical sensor by combining resonance Rayleigh scattering and colorimetry for sensitive detection of glutathione based on ultrathin MnO_2 nanoflakes. Sensors Actuators B Chem 288:195–201. https://doi.org/10.1016/j.snb.2019.02.117

21. Yan X, Song Y, Zhu CZ, Li HX, Du D, Su XG, Lin YH (2018) MnO_2 nanosheet-carbon dots sensing platform for sensitive detection of organophosphorus pesticides. Anal Chem 90:2618–2624. https://doi.org/10.1021/acs.analchem.7b04193

22. Han L, Liu SG, Zhang XF, Tao BX, Li NB, Luo HQ (2017) A sensitive polymer dots-manganese dioxide fluorescent nanosensor for "turn-on" detection of glutathione in human serum. Sensors Actuators B Chem 258:25–31. https://doi.org/10.1016/j.snb.2017.11.056

23. Huang S, Yang EL, Yao JD, Liu Y, Xiao Q (2018) Red emission nitrogen, boron, sulfur co-doped carbon dots for "on-off-on" fluorescent mode detection of Ag+ ions and l-cysteine in complex biological fluids and living cells. Anal Chim Acta 1035:192–202. https://doi.org/10.1016/j.aca.2018.06.051

24. Tian T, He Y, Ge YL, Song GW (2017) One-pot synthesis of boron and nitrogen co-doped carbon dots as the fluorescence probe for dopamine based on the redox reaction between Cr(VI) and dopamine. Sensors Actuators B Chem 240:1265–1271. https://doi.org/10.1016/j.snb.2016.09.114

25. Xiao N, Liu SG, Mo S, Li N, Ju YJ, Ling Y, Li NB, Luo HQ (2018) Highly selective detection of p-nitrophenol using fluorescence assay based on boron, nitrogen co-doped carbon dots. Talanta 184:184–192. https://doi.org/10.1016/j.talanta.2018.02.114

26. Xiao T, Sun J, Zhao JH, Wang S, Liu GY, Yang XR (2018) FRET effect between fluorescent polydopamine nanoparticles and MnO_2 nanosheets and its application for sensitive sensing of alkaline phosphatase. ACS Appl Mater Interfaces 10:6560–6569. https://doi.org/10.1021/acsami.7b18816

27. Zu FL, Yan FY, Bai ZJ, Xu JX, Wang YY, Huang YC, Zhou XG (2017) The quenching of the fluorescence of carbon dots: a review on mechanisms and applications. Microchim Acta 184:1899–1914. https://doi.org/10.1007/s00604-017-2318-9

28. Liu YN, Wang QZ, Guo SW, Jia P, Shui YH, Yao SY, Huang C, Zhang M, Wang L (2018) Highly selective and sensitive fluorescence detection of hydroquinone using novel silicon quantum dots. Sensors Actuators B Chem 275:415–421. https://doi.org/10.1016/j.snb.2018.08.073

29. Zhu RF, Huang WY, Ma XF, Zhang YH, Yue CC, Fang WH, Zhao H, Li ZX (2019) Nitrogen-doped carbon dots-V_2O_5 nanobelts sensing platform for sensitive detection of ascorbic acid and alkaline phosphatase activity. Anal Chim Acta 1089:131–143. https://doi.org/10.1016/j.aca.2019.08.061

30. Liu LZ, Mi Z, Li HH, Li CQ, Hu Q, Feng F (2019) Highly selective and sensitive detection of amaranth by using carbon dots-based nanosensor. RSC Adv 9:26315–26320. https://doi.org/10.1039/c9ra04494a

31. Liu SG, Mo S, Han L, Li N, Fan YZ, Li NB, Luo HQ (2019) Oxidation etching induced dual-signal response of carbon dots/silver nanoparticles system for ratiometric optical sensing of H_2O_2 and H_2O_2-related bioanalysis. Anal Chim Acta 1055:81–89. https://doi.org/10.1016/j.aca.2018.12.015

32. Liu SG, Li N, Han L, Li LJ, Li NB, Luo HQ (2018) Size-dependent modulation of fluorescence and light scattering: a new strategy for development of ratiometric sensing. Mater Horiz 5:454–460. https://doi.org/10.1039/c7mh00872d

33. Ren W, Zhang Y, Chen HG, Gao ZF, Li NB, Luo HQ (2016) Ultrasensitive label-free resonance Rayleigh scattering aptasensor for $Hg^{(2+)}$ using $Hg^{(2+)}$-triggered exonuclease III-assisted target recycling and growth of G-wires for signal amplification. Anal Chem 88:1385–1390. https://doi.org/10.1021/acs.analchem.5b03972

34. Li JB, Wang JH, Zhang XX, Chang HH, Wei WL (2018) Highly selective detection of epidermal growth factor receptor by multi-functional gold-nanoparticle-based resonance Rayleigh scattering method. Sensors Actuators B Chem 273:1300–1306. https://doi.org/10.1016/j.snb.2018.07.046

35. Wu ZH, Nan DY, Yang H, Pan S, Liu H, Hu XL (2019) A ratiometric fluorescence-scattered light strategy based on MoS_2 quantum dots/CoOOH nanoflakes system for ascorbic acid detection. Anal Chim Acta 1091:59–68. https://doi.org/10.1016/j.aca.2019.09.054

Publisher's note Springer Nature remains neutral with regard to jurisdictional claims in published maps and institutional affiliations.